Lithuanian Journal of Physics
Vol. **66**, No. 2, pp. 125–135 (2026)
ISSN 1648-8504 eISSN 2424-3647
DOI: https://doi.org/10.3952/physics.2026.66.2.7

STRUCTURAL AND DIELECTRIC PROPERTIES OF *TRANS*-STILBENE-TPD-TYPE MOLECULAR COMPOSITES

R. Dobužinskas [a], R. Maldžius [a], M. Solovjovaitė [a], M. Viliūnas [a], A. Poškus [a], S. Urnikaitė [b], and M. Grigalavičius [c]

[a] *Institute of Chemical Physics, Faculty of Physics, Vilnius University, Saulėtekio 3, 10257 Vilnius, Lithuania*
[b] *Department of Organic Chemistry, Faculty of Chemical Technology, Kaunas University of Technology, Radvilėnų 19, 50254 Kaunas, Lithuania*
[c] *Laser Research Center, Faculty of Physics, Vilnius University, Saulėtekio 10, 10223 Vilnius, Lithuania*
Email: rokas.dobuzinskas@ff.vu.lt

Received 27 February 2026; accepted 27 February 2026

Dedicated to Professor Vytautas Balevičius on the occasion of his 75th jubilee – for his outstanding contribution to Lithuanian physics, his long-standing pedagogical service, and the inspiration he has given to generations of students and researchers. His love for music and his ability to create a special atmosphere of togetherness have shaped those who call themselves physicists – their foundations of precision and humanity.

The crystallization behaviour and dielectric response of *trans*-stilbene embedded in a small-molecule hole-transport matrix were examined as a function of composition. In contrast to polymeric hosts, the crystallizing tritolyl-triarylamine-based material – structurally related to TPD – enables a direct analysis of mutual crystallization effects between the two molecular solids. Composite films containing 5–80% *trans*-stilbene were prepared by drop casting and characterized using X-ray diffraction, optical microscopy, and dosed charging measurements. XRD and microscopy reveal concentration-dependent phase coexistence and morphological evolution, while dielectric measurements show a pronounced nonmonotonic dependence on the composition, with an enhanced effective permittivity at intermediate concentrations (20–40%). The results highlight the interplay between molecular crystallization and interfacial polarization as a key mechanism governing and enhancing the electrostatic properties of stilbene-tolylamine intermolecular composites.

Keywords: *trans*-stilbene, hole transport materials, molecular composites, X-ray diffraction, dosed charging, dielectric permittivity

1. Introduction

Organic molecular materials play a central role in modern optoelectronic technologies, including organic light-emitting diodes, photovoltaic devices, and photodetectors [1–5]. In such systems, the microscopic arrangement of molecules critically determines charge transport, optical absorption, emission efficiency, and dielectric response. Small-molecule organic semiconductors often exhibit a strong tendency to crystallize, which can be beneficial for charge transport but detrimental to film uniformity and device stability [6–8].

Trans-stilbene is a well-known organic molecule with pronounced optical and structural properties [9–11]. In the solid state, *trans*-stilbene readily crystallizes and forms ordered domains the size and orientation of which depend strongly on processing conditions and environment. Previous studies have demonstrated that stilbene dispersed in polymeric

matrices, such as polystyrene, can exhibit the suppressed or modified crystallization, leading to the distinct optical and dielectric behaviour [12–14]. In such polymer-based systems, the host matrix is largely amorphous and does not participate in crystallization.

In contrast, a comparatively little attention has been paid to stilbene embedded in small-molecule host materials that themselves crystallize. This situation is particularly relevant for organic electronics, where hole transport layers are frequently composed of low-molecular-weight triarylamine derivatives (tuned with additional branches, e.g. tolylamine) that exhibit strong crystallization tendencies [15]. Understanding how two crystallizing molecular components influence each other is essential for controlling structure–property relationships in such systems.

In this work, stilbene is incorporated into N-TPTB, a tritolylamine-based small-molecule hole transport material structurally related to TPD (see Subsect. 2.1 for details). Both components are capable of forming crystalline phases, providing a model system for studying mutual crystallization effects in molecular composites. The aim of this study is to investigate how the concentration of *trans*-stilbene affects the crystalline structure, morphology, and dielectric response of N-TPTB-based composite films. X-ray diffraction is used to probe crystalline ordering, optical microscopy is employed to visualize domain formation, and dielectric properties are determined using the dosed charging technique.

2. Materials and methods

2.1. Materials

Trans-1,2-diphenylethylene, (*trans*-stilbene) was used as the active molecular component ordered from *Sigma-Aldrich*, CAS No. 103-30-0, purity of 96%. The host material, **N-TPTB**, is a triarylamine-based small-molecule hole transport material structurally related to the well-known compound N,N′dipheny lN,N′bis(3methylphenyl)(1,1′biphenyl)4,4′diamine (**TPD**). The naming of N-TPTB was selected to overcome duplicates with other different abbreviations of TPTB, this is the same material used in the previous work of Dobužinskas [16]. The full chemical name of N-TPTB is N,N,N′,N′tetrakis(*p*tolyl)benzidine obtained from *TCI Europe N.V.*, CAS No. 76185-65-4, purity of 98%.

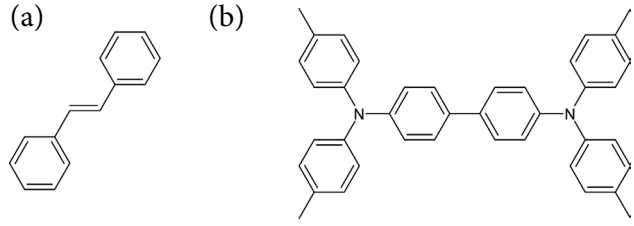

Fig. 1. Structural formulae of (a) *trans*-stilbenes and (b) N-TPTB.

2.2. Sample preparation

Composite films of *trans*-stilbene and N-TPTB were prepared using the drop-casting technique. Solutions were prepared in tetrahydrofuran (THF) containing a fixed mass of *trans*-stilbene (1.5 g) and varying amounts of N-TPTB. The mixtures were formulated to obtain *trans*-stilbene concentrations of 5, 10, 20, 40 and 80%. In this work, the stated percentages refer to the corresponding *trans*-stilbene:N-TPTB:mass ratios (e.g. 5% = 0.05:1, 10% = 0.10:1, etc.). Pure *trans*-stilbene and pure N-TPTB solutions were also prepared to serve as reference samples. Square iron-alloy substrates with dimensions of approximately 2 × 2 cm were used for film deposition. Prior to deposition, the substrates were cleaned sequentially in distilled water and acetone using an ultrasonic bath, with each step lasting 5 min. Following ultrasonic cleaning, the substrates were dried under ambient conditions. The prepared solutions were deposited onto the substrates using a pipette, and the solvent was allowed to evaporate slowly at room temperature, resulting in the formation of composite thin films.

2.3. X-ray diffraction measurements

X-ray diffraction measurements were performed using a *Rigaku* SmartLab multipurpose diffractometer equipped with a Cu sealed tube source operating at 40 kV and 50 mA. Cu K_α radiation was used, and measurements were carried out in Bragg–Brentano geometry. Diffraction patterns were collected in a continuous scan mode over the 2θ range of 5–30° with a step size of 0.01° and a scan speed of 2° min^{-1}. Diffraction peaks corresponding to *trans*-stilbene were identified and numbered using reference data from the Crystallography Open Database (COD). In addition to the *trans*-stilbene reflections, strong diffraction maxima attributable to N-TPTB were also

observed; however, because this material is not yet established within industry and no validated reference diffraction pattern is available, the assignment of these reflections remains provisional.

2.4. Optical microscopy

Film morphology was examined using an OLYMPUS BX41 optical microscope equipped with a PixelINK PL-B623 digital camera under both polarized and non-polarized illumination. Images were collected at locations selected to capture the dominant patterns present within each sample. Multiple regions were examined to ensure a representative assessment of the film surface.

2.5. Dosed charging measurements

The dielectric properties of the composite films were investigated using a dosed-charging technique based on the repetitive corona charge deposition and measurement of the resulting surface potential [17]. The sample was placed on a rotating disk, undergoing sequential charging and potential-measurement stages during each revolution. The deposited charge was determined from the electric current flowing through the base electrode during electrification, while the surface potential was measured using a noncontact Kelvin probe. For each rotation, the charge and potential values were recorded over time, producing the corresponding kinetic curves. Charging cycles were repeated until an equilibrium surface potential was reached, indicating a steady balance between charge deposition and leakage through the film.

From the charge-potential kinetics, the effective capacitance can be determined by dividing the charge dose delivered during each cycle by the corresponding increase in surface potential. The dielectric permittivity of the film is proportional to this effective capacitance when the potential is close to zero; therefore, the permittivity is obtained by extrapolating the capacitance of the first charging cycle to $U \to 0$ and using an independent measurement of the film thickness d

$$\varepsilon = \frac{d}{S\varepsilon_0} C(U)\,|_{U\to 0}, \tag{1}$$

where S is the square area of the film.

Accurate determination of the film's relative permittivity requires an independent measurement of the film thickness. In this work, the thickness was measured mechanically using a micrometer with a precision of approximately one micron. The layer thickness was recorded at nine different locations across the sample surface, and the resulting values were averaged. If the thickness is difficult to determine or remains unknown, the dielectric response can instead be expressed as the permittivity normalized by the film thickness, $\varepsilon_{\text{norm}} = \varepsilon/d$. This normalized permittivity also characterizes the dielectric properties of the layer and is useful for analysing not only composite films but also multilayer structures [18].

It is important to note that the dielectric permittivity is calculated from the first charge dose (i.e. at the limit of $U \to 0$) and therefore provides the closest estimate of the intrinsic dielectric permittivity of the layer. This is because the geometric capacitance of the layer is charged before significant effects of surface charge injection–extraction or bulk polarization begin to manifest. The nonlinearity observed in the initial part of the effective-capacitance kinetics reflects the onset of charge injection and extraction processes, while the sharp rise in the final stage indicates the onset of charge transport through the film. The potential at which this through-layer charge flow begins is referred to as the limiting charging potential of the film. Typically, materials with higher dielectric constants exhibit higher limiting charging potentials [19, 20].

3. Results

3.1. X-ray diffraction analysis

The concentration-dependent structural evolution of the *trans*-stilbene/N-TPTB composites was examined using X-ray diffraction, and the corresponding patterns for all investigated compositions are presented in Fig. 2.

In the low-stilbene region (0–10%), the diffraction patterns are dominated by a reflection at $2\theta \approx 10.7°$, which remains fixed in position across all compositions. The increased intensity and sharper profile of this peak at 5–10% stilbene indicate an improved structural coherence within the unchanged N-TPTBlike packing. No additional

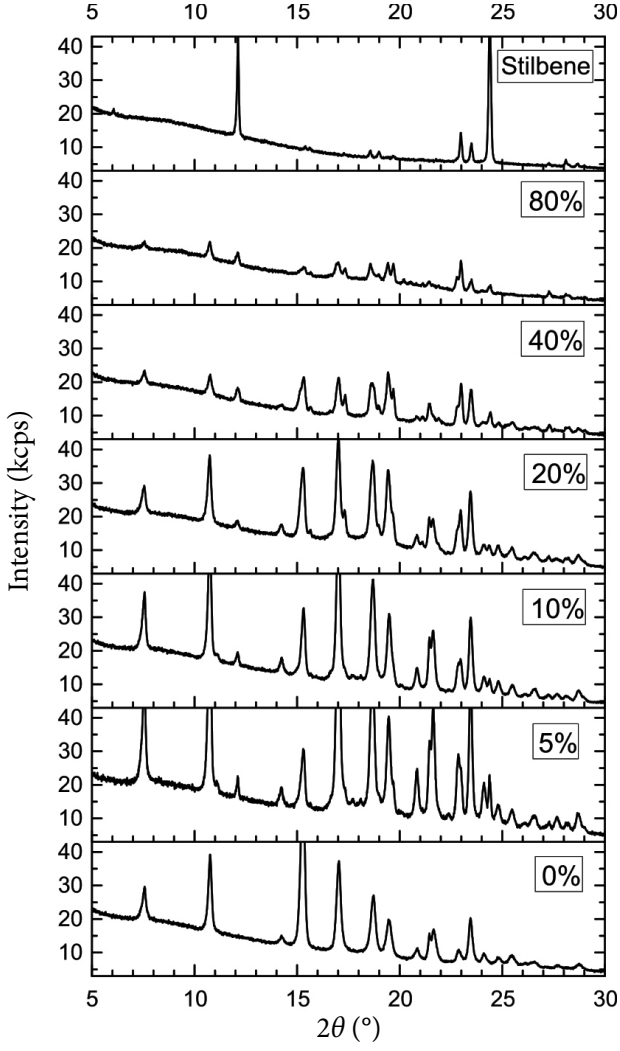

Fig. 2. X-ray diffraction measurements performed for pure *trans*-stilbene, pure N-TPTB (labelled as 0%) and *trans*-stilbene different concentrations (5, 10, 20, 40 and 80%). Intensities are reported in kcps (kilocounts per second).

major reflections appear in this range, showing that small stilbene additions do not modify the fundamental structure.

Increasing the concentration to around 20% results in a noticeable reduction in both intensity and sharpness of the 10.7° reflection. Although the peak is still present, its broadening signals the onset of structural reorganization and a gradual loss of coherence within the original packing motif. Subtle changes in weaker reflections and background shape also emerge, marking this composition as a transitional point between the low-stilbene and high-stilbene structures.

With a further increase to 40% stilbene and above, the diffractograms undergo a pronounced transformation. The reflection at 10.7° is no longer dominant and is drastically reduced, together with the low-angle reflection at 7.6° that is characteristic of NTPTB. At the same time, the peak associated with stilbene at 12.0° emerges and remains stable for both the 40 and 80% samples. This behaviour indicates the formation of a stilbene-rich lamellar arrangement that replaces the original N-TPTB-like structure.

Throughout the entire concentration series, several smaller reflections at intermediate angles remain visible, including those around the 17° region. These features show only minor variation with composition and are characteristic of internal molecular repeats common to both structural motifs. They are therefore not indicators of the main structural transition, which is defined primarily by the evolution of the 7.6, 10.7 and 12.0° reflections.

3.2. Morphological characterization

In the high-stilbene samples, the optical micrographs reveal distinct crystalline textures with a strong contrast under polarized illumination. Pure *trans*-stilbene, Fig. 3(a–b), exhibits elongated, brightly coloured birefringent domains, indicative of a well-developed crystalline order. At 80 and 40% stilbene, Fig. 3(c–f), the films retain visible crystalline regions, though the domains become more fragmented and less directional. Under cross-polarization, these compositions still display scattered bright features, confirming the presence of birefringent crystallites dispersed within the film.

At intermediate concentrations of 20 and 10% stilbene, Fig. 3(g–j), the films transition toward more uniform and finer-grained morphologies. Only isolated bright spots appear under cross-polarised light, indicating that larger birefringent crystals are largely suppressed. At 5% stilbene, Fig. 3(k–l), the films appear almost featureless in both illumination modes, suggesting a predominantly homogeneous microstructure with a minimal optically detectable crystallinity. Pure N-TPTB, Fig. 3(m–n), shows a slightly mottled texture with a weak birefringence, consistent with small, irregular ordered domains characteristic of this material.

The sequence of images demonstrates a clear concentration-dependent reduction in crystalline domain size and birefringence as the amount of *trans*-stilbene decreases. Highly ordered crystalline textures dominate at high stilbene content, while

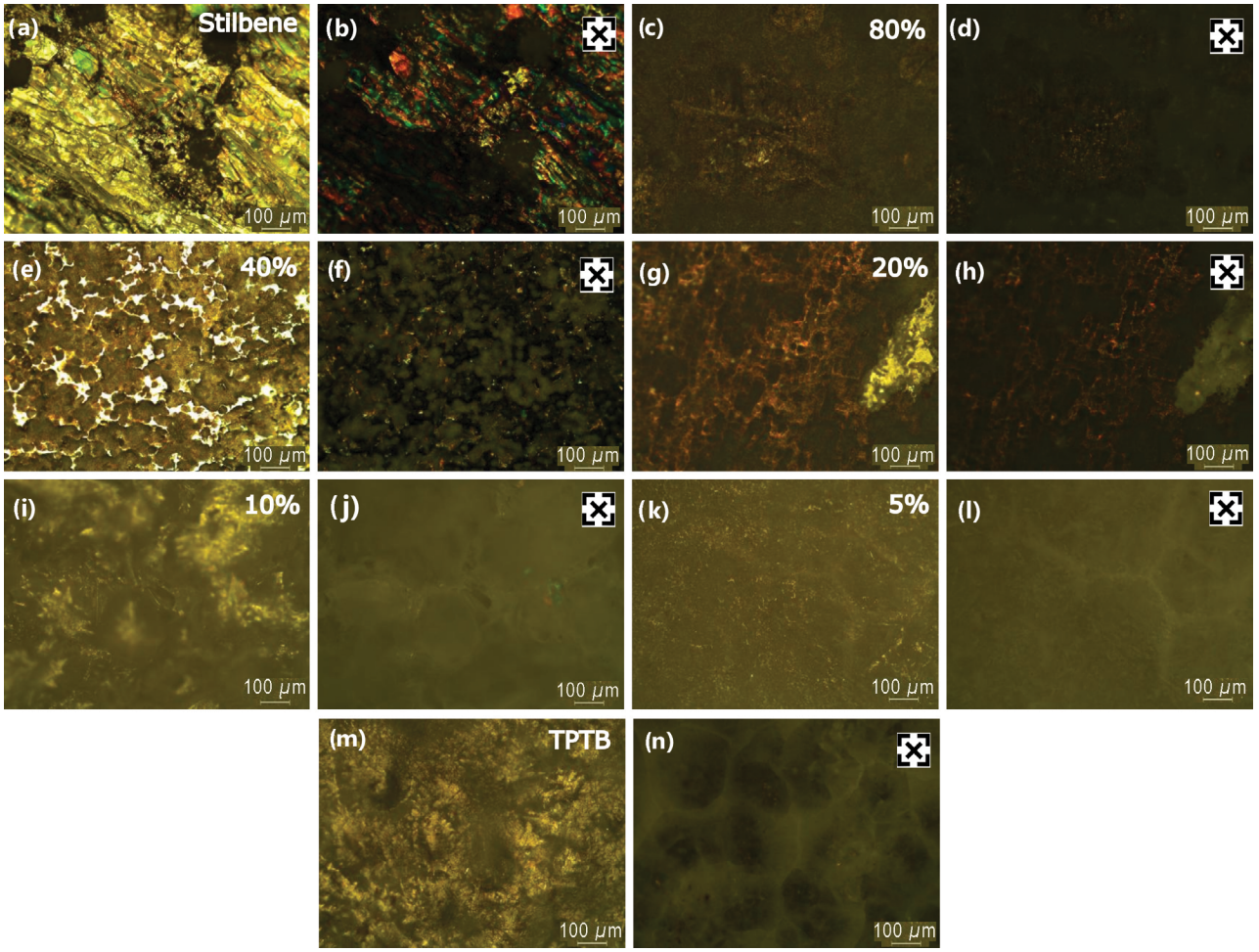

Fig. 3. Optical microscopy images of *trans*-stilbene/N-TPTB composite films, shown under polarized (left) and cross-polarized (right, '[×]') illumination. Samples correspond to (a–b) pure *trans*-stilbene, (c–d) 80%, (e–f) 40%, (g–h) 20%, (i–j) 10%, (k–l) 5% and (m–n) pure N-TPTB.

intermediate compositions exhibit mixed morphologies with diminishing birefringent regions. At low stilbene levels, the films appear largely amorphous or finely dispersed, and pure N-TPTB shows only weak structural ordering. This progression indicates that stilbene strongly promotes crystalline domain formation within the composite, and its dilution leads to a continuous suppression of long-range order in favour of more uniform, low-contrast microstructures.

3.3. Dielectric properties

To assess the dielectric behaviour of the *trans*-stilbene/N-TPTB composites, corona-charging measurements were carried out to record the evolution of surface potential and the corresponding capacitance–voltage characteristics for each film. These measurements provide two complementary outputs: time-dependent charging curves reflecting the film's ability to accumulate charge under unipolar corona exposure, and C–V dependences from which the effective capacitance and apparent permittivity are extracted. Because the corona method probes the combined response of the film, its thickness and internal interfaces, the resulting dielectric parameters represent effective values influenced by both material properties and geometry. The measured charging and C–V curves are presented in Fig. 4.

The corona-charging measurements reveal systematic differences in the charging behaviour of the composite films across the concentration series. Pure stilbene, 80 and 40% samples exhibit a rapid potential build-up and reach high limiting potentials within several seconds, reflecting their relatively thin films and an efficient charge uptake. In contrast, the 20, 10 and especially 5% compositions

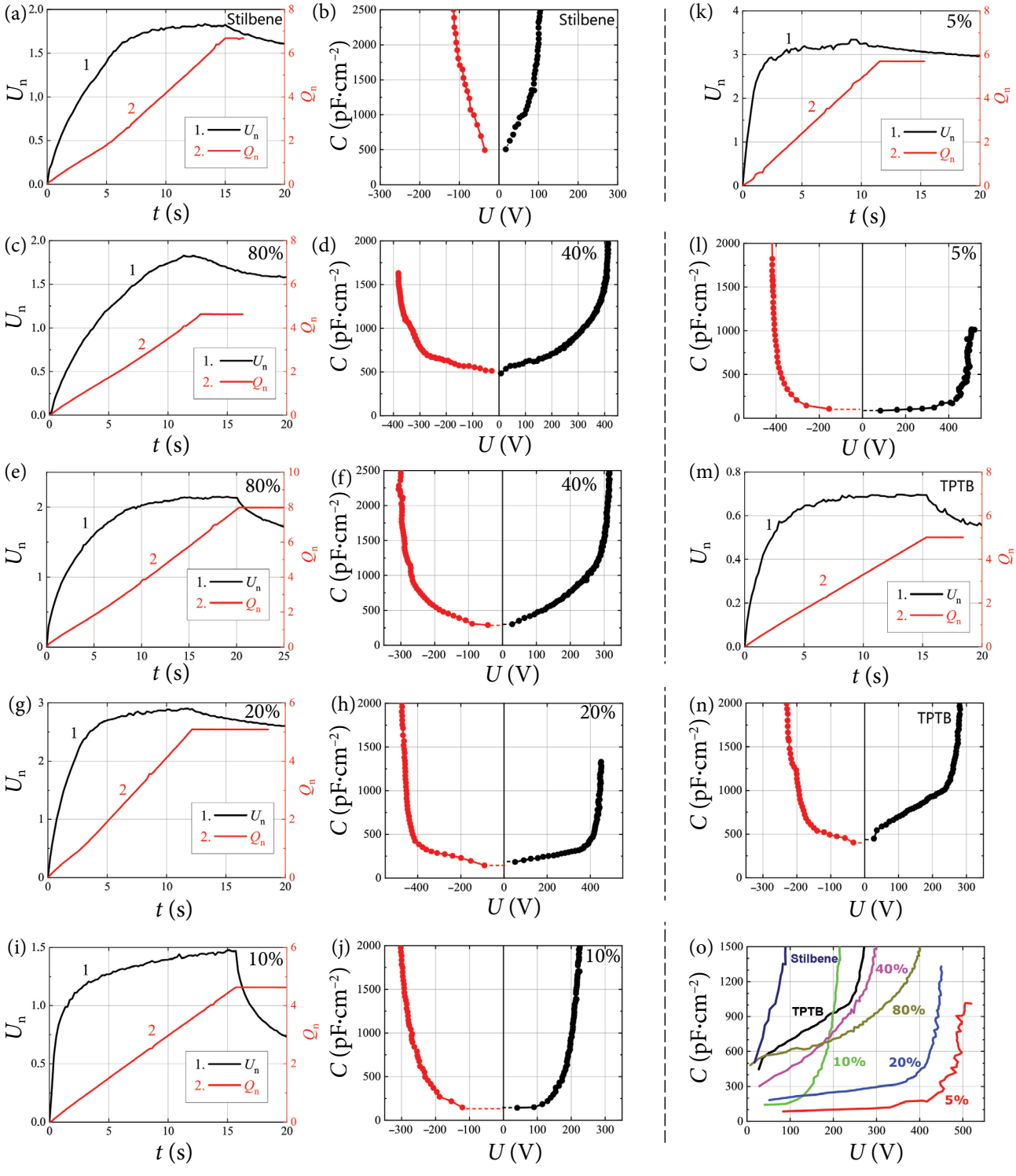

Fig. 4. Dosed charging characteristics of N-TPTB/*trans*-stilbene composite films at different *trans*-stilbene concentrations. Samples shown are (a–b) pure *trans*-stilbene, (c–d) 80%, (e–f) 40%, (g–h) 20%, (i–j) 10%, (k–l) 5% and (m–n) pure N-TPTB. For each concentration, charge-kinetics data are followed by the corresponding capacitance–voltage characteristics. All positive-polarity capacitance–voltage curves are compiled together in the final overlay panel (o).

display a slower and weaker potential growth, consistent with their larger thicknesses and reduced charging efficiency. Pure N-TPTB shows the intermediate behaviour with a smooth rise in the surface potential. Across the series, both the slope of the charging curve and the final limiting potential vary with composition, indicating that the microstructure and geometry of the films

strongly influence their ability to accumulate and retain surface charge.

The capacitance–voltage plots in the right-hand panels (Fig. 4) provide the quantitative basis for determining the effective capacitance of each film. In these measurements, capacitance is obtained directly from the slope of the $Q(U)$ curves at sufficiently slow charging rates, and is read from the potential-dependent $C(U)$ traces shown for each composition. Stilbene-rich films (pure, 80 and 40%) exhibit large capacitances throughout most of the voltage range, whereas the 20 and 10% samples show a lower, more gradually varying capacitance. The lowest values appear in the 5% and pure-N-TPTB films, where the $C(U)$ curves are comparatively flat, consistent with a weaker polarizability and the thicker, more uniform morphology revealed by microscopy.

The dielectric parameters of the films calculated from the experimental curves are shown in Table 1. The effective dielectric permittivity of the *trans*-stilbene/N-TPTB composites exhibits a strong, non-monotonic dependence on composition. At low stilbene concentrations, the permittivity decreases significantly, reaching a minimum at 10%, indicating a dielectric response dominated by the N-TPTB matrix with a limited polarization contribution from stilbene. With increasing stilbene content, the permittivity increases markedly and reaches a maximum at intermediate concentrations of 20–40%.

The measured capacitance varies strongly with film thickness, and this geometric effect must be considered before interpreting compositional trends. Because capacitance scales inversely with thickness ($C \propto 1/d$), the thinner films at high stilbene content (25–35 μm) naturally exhibit larger capacitances, while the thicker low-stilbene films (80–100 μm) show correspondingly reduced values even when their intrinsic permittivity is not lower. When the thickness-corrected permittivity values are examined, a nonmonotonic dependence on stilbene concentration emerges: low concentrations (≤10%) yield modest ε values characteristic of a predominantly N-TPTB-like matrix, intermediate mixtures (20–40%) show enhanced permittivity consistent with increased internal heterogeneity, and high stilbene fractions (80–100%) recover large ε values associated with thin, polarizable stilbene-rich films.

Figure 5 compiles the concentration-dependent dielectric parameters extracted from the corona-charging experiments and summarized in Table 1, presenting both the effective permittivity and the limiting potential as a function of *trans*-stilbene content. The permittivity values display a distinctly nonmonotonic trend, rising from the low-stilbene region to a maximum at intermediate and high stilbene fractions, while the limiting potential shows an opposite evolution, decreasing as stilbene becomes the dominant component of the composite. For comparison, the curve labelled 'equivalent' shows the permittivity predicted by the Lichtenecker–Rother mixing formula, calculated using the individual permittivity of pure N-TPTB and pure stilbene. The experimental data for the composite films follow this mixing line only partially: compositions around 40 and 80% stilbene yield permittivity that exceed the predicted values, whereas deviations remain within the uncertainty associated with thickness variations. This comparison highlights that the measured dielectric response cannot be

Table 1. Dielectric parameters of N-TPTB and *trans*-stilbene composites at different *trans*-stilbene concentrations.

trans-stilbene concentration in N-TPTB, %	Mass proportion, stilbene: N-TPTB	Limiting potential, V	$C(t)\|_{t\to 0}$, pF/cm^2	Dielectric permittivity, ε, a.u.	Thickness, mm
Pure N-TPTB	0 : 1	270	400	6.8	15
5%	0.048 : 0.952	450	85	9.6	100
10%	0.091 : 0.909	200	90	8.1	80
20%	0.167 : 0.833	400	157	6.2	35
40%	0.286 : 0.714	300	280	10.4	33
80%	0.444 : 0.556	400	480	15.2	28
Pure stilbene	1 : 0	100	500	14.1	25

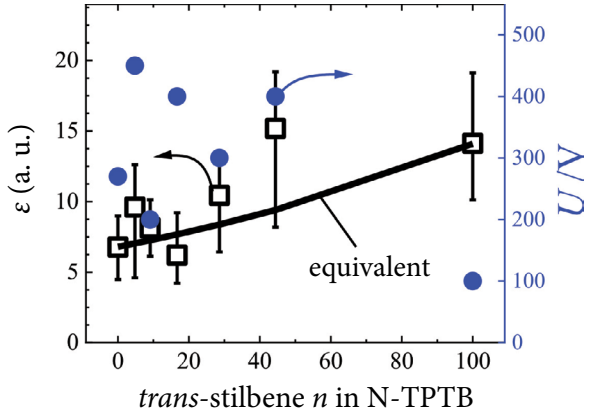

Fig. 5. Dielectric permittivity ε (left scale) and limiting potential *U* (right scale) of N-TPTB/*trans*-stilbene composite films at different *trans*-stilbene concentrations. The curve labelled 'equivalent' represents values calculated using the Lichtenecker–Rother mixing formula [12].

explained solely by volume averaging and instead reflects additional microstructural and interfacial contributions that are addressed in the subsequent discussion.

4. Discussion

The optical microscopy images and the XRD patterns show the same concentration-dependent structural evolution, each from a different perspective. At high *trans*-stilbene content, the microscopy reveals large, well-defined birefringent crystalline domains, especially in the pure and 80% stilbene samples. This correlates directly with the XRD results, where the 10.7° N-TPTB-like reflection is strong together with the low-angle 7.6° and the appearance of 12° peak indicates distinct layered crystalline arrangements characteristic of stilbene-rich compositions.

As the stilbene content decreases to 40 and 20%, the microscopy shows mixed morphologies with granular or partially disrupted crystalline regions. This matches the XRD transition zone, where the 10.7° peak weakens and broadens while the new low-angle reflections begin to emerge. Both techniques capture a coexistence of multiple packing motifs, consistent with partial phase reorganization.

At a low stilbene content (10 and 5%), the optical images appear uniform and nearly featureless, with essentially no birefringence. This is fully consistent with the XRD data, where the lamellar stilbene peaks disappear and the N-TPTB-like peak dominates but with reduced coherence. Pure N-TPTB exhibits a slightly textured, weakly birefringent appearance, in line with its XRD pattern showing small, disordered domains. Altogether, the microscopy and XRD results provide a coherent picture of a progressive loss of stilbene-driven crystallinity and a shift from ordered lamellar structures toward amorphous or finely dispersed morphologies as the stilbene fraction decreases.

The combined structural, morphological and dielectric results demonstrate that the electrical response of *trans*-stilbene/N-TPTB composites is governed by the interplay between molecular crystallization and interfacial effects. Intermediate compositions appear to promote the formation of interconnected stilbene-rich domains within the N-TPTB matrix, enhancing polarization and charge storage capabilities. In contrast, low and high stilbene concentrations lead to less favourable structural arrangements that limit an effective dielectric response.

To interpret the dielectric behaviour of the *trans*-stilbene/N-TPTB composite films, it is important to note that the measured capacitance and the resulting effective permittivity depend not only on intrinsic material properties but also on the film thickness and microstructural heterogeneity. Variations in stilbene concentration lead to systematic changes in morphology – from uniform, low-contrast films at a low stilbene content to increasingly interconnected and eventually highly crystalline domains at higher concentrations – and these structural transformations strongly influence charge accumulation, interfacial polarization, and the field distribution within the films. Because the dosed-charging method senses the overall response of the film-substrate stack, thinner and more polarizable films naturally exhibit a higher apparent capacitance, while thicker or more weakly ordered samples display lower values. Consequently, the extracted dielectric permittivity reflects both composition-dependent polarization mechanisms and geometric factors, and should therefore be viewed as an effective parameter that captures the combined influence of microstructure, interfaces, and thickness variations across the series. The concentration-dependent dielectric response of *trans*-stilbene/N-TPTB composites can be rationalized by considering interfacial (Maxwell–Wagner–Sillars) polarization, microstructural percolation,

and trap-assisted charge dynamics under corona charging. At a low stilbene content (≤10%), the composite is dominated by N-TPTB domains with dispersed stilbene molecules; the limited number and continuity of stilbene-rich interfaces suppress interfacial polarization, yielding a low effective permittivity. At intermediate compositions (20–40%), stilbene-rich domains become sufficiently interconnected to form extended interfaces with the N-TPTB matrix. These heterogeneous boundaries support charge accumulation and polarization at differing local conductivities and permittivity, enhancing the effective dielectric response. Simultaneously, the partial percolation of stilbene-rich pathways improves the field-assisted dipolar alignment without fully crystallizing into large, defect-laden grains. At a high stilbene content (≈80%), the excessive crystallite growth and aggregation introduce internal barriers and trap states at grain boundaries. Corona-deposited charges increasingly undergo trap-assisted leakage and non-uniform potential build-up, reducing the net polarization efficiency and thereby the effective permittivity. The non-monotonic $\varepsilon(n)$ trend observed here is therefore consistent with a competition between (i) beneficial interfacial polarization at composite heterojunctions and (ii) detrimental charge trapping and microstructural discontinuities once large stilbene crystallites dominate. Finally, because the dosed charging method senses the total capacitance of the film-substrate stack, thickness variations and interfacial layers contribute to the measured dielectric permittivity values. This motivates reporting ε as an effective quantity and focusing on robust compositional trends; conversion to ε_r is feasible once thickness and geometry are independently validated.

Using the Lichteneker and Rother formula $\ln \varepsilon = V_1 \ln \varepsilon_1 + V_2 \ln \varepsilon_2$ to calculate the dielectric constant of two media for granular materials and their mixtures [21], we can evaluate the equivalent dielectric permittivity for our film when we know the individual dielectric permittivity values of stilbene and N-TPTB materials separately. Here V_1 and V_2 are the volumes of the first and second media ($V = V_1 + V_2$), and ε_1 and ε_2 are the permittivity values accordingly. The curve for such a calculation is shown as a solid line in Fig. 5 and is called the equivalent dielectric permittivity of the mixture film. We see that the permittivity of our films with stilbene concentrations of 40 and 80% little separates from the calculated curve and the values are higher, although they do not exceed the error limits calculated by varying the thickness of the layers.

Despite the scatter observed for the 20 and 40% stilbene compositions, the results in Fig. 5 indicate that the limiting charging potential decreases monotonically with increasing stilbene content. This behaviour is somewhat unexpected when viewed alongside the relatively high permittivity values of these films. A higher permittivity would normally suggest an improved polarization and therefore a greater ability to sustain the surface potential; however, the opposite trend appears here, implying that charge carriers increasingly find conductive or semiconductive pathways through the microstructure as stilbene content rises. These pathways reduce the effective ability of the layer to retain charge and therefore lower the limiting potential. The microscopy images support this interpretation: films with more pronounced granular morphologies contain interconnected structural features that can facilitate charge transport, allowing injected carriers to bypass the bulk polarization and reach the substrate more readily.

5. Conclusions

The results demonstrate that *trans*-stilbene/N-TPTB composites exhibit a clear composition-driven evolution of structure, morphology, and dielectric behaviour, forming a coherent structure–property relationship. At low stilbene levels, the films retain a N-TPTB-like packing and weak morphological ordering, which correlates with reduced permittivity. Intermediate compositions (20–40%) mark the emergence of heterogeneous, partially interconnected stilbene-rich domains that maximize interfacial polarization and yield the highest effective dielectric response. At higher stilbene contents, lamellar stilbene phases dominate and enhance intrinsic polarizability, although the increasing grain-boundary pathways lower the limiting charging potential. Together, these findings show that the interplay between molecular crystallization, microstructural heterogeneity, and charge-accumulation dynamics governs the dielectric performance of this binary system, with intermediate compositions offering the most favourable balance of structural order and interfacial effects.

Acknowledgement

This project has received funding from the Research Council of Lithuania (LMTLT), Agreement No. S-MIP-25-20.

References

[1] C.W. Han and Y.H. Tak, OLED manufacturing process for TV application, in: *Flat Panel Display Manufacturing* (John Wiley & Sons, Ltd, 2018).

[2] N.S. Sariciftci, D. Braun, C. Zhang, V.I. Srdanov, A.J. Heeger, G. Stucky, and F. Wudl, Semiconducting polymer-buckminsterfullerene heterojunctions: Diodes, photodiodes, and photovoltaic cells, Appl. Phys. Lett. **62**, 585(1993).

[3] K. Zhang, J. Wu, C. Sun, D.S. Chung, Y. Geng, and L. Ye, The rising promise of organic photodetectors in emerging technologies, Nat. Rev. Mater. **10**, 487 (2025).

[4] R. Dobužinskas, A. Poškus, V. Jankauskas, M. Viliūnas, E. Kamarauskas, M. Daškevičienė, V. Getautis, K. Arlauskas, and D. Abramavičius, Bromine-enhanced organic materials for X-ray sensors: Unveiling the potential of small molecules and polymers through material design and film fabrication, Adv. Sensor Res. **3**, 2400018 (2024).

[5] R. Dobužinskas, A. Poškus, M. Viliūnas, V. Jankauskas, M. Daškevičienė, V. Getautis, and K. Arlauskas, Melt spin coating for X-ray-sensitive hybrid organic-inorganic layers of small carbazoly-containing molecules blended with tungsten, Phys. Status Solidi A **216**, 1900635 (2019).

[6] C. Garcias-Morales, D. Romero-Borja, J.-L. Maldonado, A. Roa, M. Rodríguez, J. García-Merinos, and A. Ariza-Castolo, Small molecules derived from Thieno[3,4-c]pyrrole-4,6-dione (TPD) and their use in solution processed organic solar cells, Molecules **22**, 1607 (2017).

[7] G. Juška, K. Arlauskas, and K. Genevičius, Charge carrier transport and recombination in disordered materials, Lith. J. Phys. **56**, 182 (2016).

[8] A. Intaniwet, J.L. Keddie, M. Shkunov, and P.J. Sellin, High charge-carrier mobilities in blends of poly(triarylamine) and TIPS-pentacene leading to better performing X-ray sensors, Org. Electron. **12**, 1903 (2011).

[9] M. Kluska, J. Jabłońska, and W. Prukała, Analytics, properties and applications of biologically active stilbene derivatives, Molecules **28**, 4482 (2023).

[10] G.I. Likhtenshtein, *Stilbenes: Applications in Chemistry, Life Sciences and Materials Science* (Wiley, 2009).

[11] V. Govindan, D.J. Daniel, P.Q. Vuong, K. Sankaranarayanan, and H.J. Kim, Unidirectional growth of pure and composite t-stilbene single crystals for scintillator applications, J. Cryst. Growth **531**, 125344 (2020).

[12] I. Halimski, R. Karpicz, A. Dementjev, M. Jankunec, J. Chmeliov, M. Macernis, D. Abramavicius, and L. Valkunas, *trans*-Stilbene aggregates and crystallites in polystyrene films: microscopy and spectroscopy studies, Phys. Chem. Chem. Phys. **26**, 23692 (2024).

[13] N. Zaitseva, A. Glenn, L. Carman, H.P. Martinez, R. Hatarik, H. Klapper, and S. Payne, Scintillation properties of solution-grown *trans*-stilbene single crystals, Nucl. Instrum. Methods Phys. Res. A **789**, 8 (2015).

[14] J. Bernstein, Refinement of *trans*-stilbene: A comparison of two crystallographic studies, Acta Crystallogr. B **31**, 1268 (1975).

[15] M. Nagai and H. Nozoye, Crystallization and aggregation processes of vacuum-evaporated TPD films, J. Electrochem. Soc. **154**, J239 (2007).

[16] R. Dobužinskas, A. Poškus, and K. Arlauskas, X-ray sensitivity of small organic molecule and zinc cadmium sulfide mixture layers deposited using thermal melting technique, Org. Electron. **18**, 37 (2015).

[17] P. Sirviö, J. Sidaravicius, T. Lozovski, S. Kuskevicius, and K. Backfolk, Dosed charging: Application to the investigation of papers, J. Electrost. **67**, 730 (2009).

[18] R. Maldzius, T. Lozovski, J. Sidaravicius, K. Backfolk, and I. Heiskanen, Influence of environmental relative humidity on the polarization behaviour of paper and paper-dielectric structures, Cellulose **27**, 10303 (2020).

[19] P. Hofmann, *Solid State Physics: An Introduction* (Wiley, 2015).

[20] D.J. Griffiths, *Introduction to Electrodynamics* (Cambridge University Press, 2023).

[21] G.G. Raju, *Dielectrics in Electric Fields: Tables, Atoms, and Molecules*, 2nd ed. (CRC Press, Boca Raton, 2017).

TRANS-STILBENO IR TPD TIPO MOLEKULINIO KOMPOZITO STRUKTŪRINĖS IR DIELEKTRINĖS SAVYBĖS

R. Dobužinskas [a], R. Maldžius [a], M. Solovjovaitė [a], M. Viliūnas [a], A. Poškus [a], S. Urnikaitė [b], M. Grigalavičius [c]

[a] *Vilniaus universiteto Fizikos fakulteto Cheminės fizikos institutas, Vilnius, Lietuva*

[b] *Kauno technologijos universiteto Cheminės technologijos fakulteto Organinės chemijos katedra, Kaunas, Lietuva*

[c] *Vilniaus universiteto Fizikos fakulteto Lazerinių tyrimų centras, Vilnius, Lietuva*

Skiriama profesoriui Vytautui Balevičiui, mininčiam 75 metų jubiliejų – už išskirtinį indėlį į Lietuvos fizikos mokslą, ilgametę pedagoginę tarnystę ir įkvėpimą, kurį suteikė kelioms kartoms studentų bei tyrėjų. Jo meilė muzikai ir gebėjimas kurti ypatingą bendrystės atmosferą formavo tuos, kurie save vadina fizikais, – jų tikslumo ir žmogiškumo pamatus.

Santrauka

Šiuo tyrimu pristatomas *trans*-stilbeno kristalizacijos ir dielektrės skvarbos sąryšis, įterpiant į mažos molekulinės masės skylių pernašos matricą TPD tipo mažamolekulinę medžiagą N-TPTB. Skirtingai nei polimerai, N-TPTB yra linkęs kristalizuotis dėl tritolilo-triarilamino funkcinių grupių, kurios struktūriškai artimos TPD, tačiau kristalizacijos efektas išreikštas maksimaliu chemiškai struktūriniu būdu. Tokiu būdu sistema leidžia nagrinėti maksimaliai išreikštus tarpusavio kristalizacijos reiškinius tarp dviejų molekulinių kietųjų fazių. Buvo pagaminti ir ištirti kompoziciniai plėveliniai mėginiai, turintys 5–80 % *trans*-stilbeno, panaudojant liejimo iš tirpalo metodą. Jų struktūrinės ir fizikinės savybės analizuotos rentgeno difrakcijos, optinės mikroskopijos ir dozuoto įkrovimo metodais. Rentgeno difrakcija ir mikroskopija atskleidė koncentracijai jautrų fazių koegzistavimą ir mikrostruktūros kitimą, o dielektriniai matavimai parodė ryškų nemonotonišką priklausomybės nuo sudėties pobūdį: efektyviausia dielektrinė skvarba įvertinta tarpiniuose mišiniuose (20–40 %). Rezultatai rodo, kad molekulinės kristalizacijos ir tarpfazių poliarizacijos tarpusavio sąveika yra pagrindinis mechanizmas, lemiantis ir stiprinantis elektrostatines stilbeno-tolilamino kompozitų savybes.